Available online at www.sciencedirect.com
ScienceDirect
Nuclear Physics B Proceedings Supplement 00 (2013) 1–8
Nuclear Physics B Proceedings Supplement

Precision QCD measurements at HERA: Jet production and α_S determination

Stanislaw Mikocki on behalf the H1 and ZEUS Collaborations

Institute of Nuclear Physics PAN, Radzikowskiego 152, 31-342 Kraków, Poland

Abstract

A review of recent high precision measurements of inclusive-jet, dijet and trijet production in deep-inelastic scattering and photoproduction at HERA is presented. The data are compared to NLO QCD prediction. The measurements are used to extract the value of the strong coupling $\alpha_S(M_Z)$. Also, the test of QCD evolution mechanisms using the azimuthal correlation between the most forward jet and the scattered positron is presented.

Keywords: deep-inelastic scattering, jet production, quantum chromodynamics, strong coupling, BFKL

1. Introduction

The HERA electron-proton collider is an excellent testing ground for QCD calculations in next-to-leading order (NLO) of the strong coupling α_S and offers the possibility of a precise determination α_S. Despite of the HERA shutdown in 2007, the collider experiments H1 and ZEUS continue to provide new precise results. At HERA, jet production can be studied in two regimes of the exchanged boson virtuality Q^2: deep-inelastic scattering (DIS) for $Q^2 > 1$ GeV^2 and photoproduction for $Q^2 \sim 0$ GeV^2. In the following, results on jet production and the extraction of α_S in both regimes are reviewed. Tests of different QCD evolution mechanisms using azimuthal correlations between the most forward jet (i.e. close to proton direction) and the scattered positron in DIS are also presented.

2. Multi-jet production in DIS

Jet production in neutral current (NC) DIS provides an important testing ground for QCD. While inclusive DIS only gives indirect information on the strong coupling via scaling violations of the proton structure functions, jet production in the Breit frame is directly sensitive to α_S. The Born level contribution to DIS generates no transverse momentum in the Breit frame, where the virtual boson and proton collide head on. Significant transverse momentum P_T is produced at leading order (LO) in the strong coupling α_S by the QCD-Compton (QCDC) and boson-gluon fusion processes (BGF). In the kinematic regions of low Q^2, low P_T or low ξ (where ξ is the momentum fraction of proton carried by the parton entering the hard process), BGF dominates jet production and provides direct sensitivity to the gluon component of Parton Distribution Functions (PDFs) and to α_S. At high Q^2 and high P_T QCDC processes are dominant, which are sensitive to the valence quark distributions and α_S. Therefore, in the extraction of PDFs, the inclusion of jet production is expected to provide important constraints on α_S and allows the correlation between α_S and the gluon to be disentangled.

2.1. Jet production at high Q^2

The high Q^2 measurement of the jet cross sections in DIS presented here [1] is based on data with an integrated luminosity of 361pb^{-1} collected in the years 2003-2007 with the H1 detector. The NC DIS events are selected in the phase space: $150 < Q^2 < 15000$ GeV^2 and $0.2 < y < 0.7$. Jet finding is performed in Breit frame using the inclusive k_T algorithm as implemented in FastJet [2], with the massless P_T recombination scheme and with distance parameter $R_0 = 1$. The jet pseudorapidity in the laboratory frame is restricted to $-1.0 < \eta_{lab} < 2.5$. All jets with transverse momentum

P_T in the Breit frame satisfying $7 < P_T < 50$ GeV contribute to the inclusive jet cross sections. Events with at least two (three) jets fulfilling the requirement $5 < P_T < 50$ GeV and $M_{12} > 16$ GeV, where M_{12} is the invariant mass of the two leading jets of highest P_T are considered as dijet (trijet) events. The measured inclusive, dijet and trijet cross sections as a function of P_T (the average transverse momentum $\langle P_T \rangle$ in case of the dijet and trijet measurements) are shown in Figure 1 and are compared to NLO predictions on hadron level. The precision is improved by a factor $2-3$ compared to a previous H1 measurement, mainly due to the use of a larger event sample and an improved hadronic energy scale uncertainty of 1%. The QCD NLO predictions provide a good description of the data. The theory error, dominated by the renormalisation scale uncertainty, is significantly larger than the total experimental uncertainty, which is dominated by the uncertainty due to the model dependence of the data correction and the hadronic energy scale uncertainty. The trijet cross sections are already at Born level proportional to α_S^2 and the NLO calculations then include terms of $O(\alpha_S^3)$. Thus the trijet cross sections provide an important test of perturbative QCD. The data are well described by the NLO calculation. The experimental uncertainties are larger than in the dijet case, due to a large uncertainty originating from the model dependence but are still smaller than the theoretical uncertainty.

The normalised inclusive, dijet and trijet cross sections as function P_T ($\langle P_T \rangle$ for dijet and trijet) and Q^2 are shown in Figure 2 and are compared to NLO predictions on hadron level. The advantages of the normalisation to the inclusive DIS measurement is a reduction of experimental systematic uncertainties as well as a reduction of PDF uncertainties. The obtained jet cross sections are determined using a regularised unfolding procedure which also provides the full correlation matrix of all inclusive jet, dijet, and trijet measurements. The NLO calculations provide a good description of the measurements. The experimental uncertainties are smaller than theoretical ones with the exception of the highest Q^2 bins.

The value of $\alpha_S(M_Z)$ is extracted from a simultaneous fit to the normalised jet cross sections. In order to ensure that the observables have a small dependence on missing higher orders, the fit is restricted to the bins with k-factor $k < 1.3$ where the k-factor is defined as the ratio of the cross section calculated in NLO and LO, $k = \sigma_{NLO}/\sigma_{LO}$. It is used as an indicator for missing higher orders in the QCD calculation. The resulting

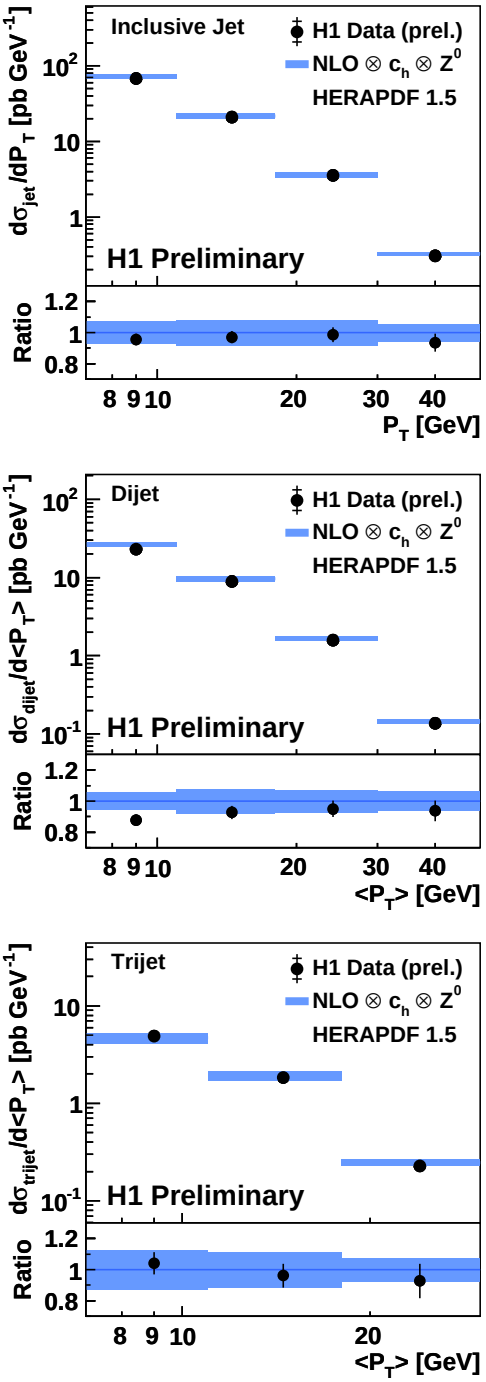

Figure 1: Inclusive jet, dijet and trijet cross sections as functions of transverse momentum of the leading jet in the Breit frame P_T (or average transverse momentum of the leading jets $\langle P_T \rangle$). The NLO QCD predictions are corrected for hadronisation effects and are shown with the theory uncertainties (shaded band). The ratios of data to the NLO QCD prediction are also shown.

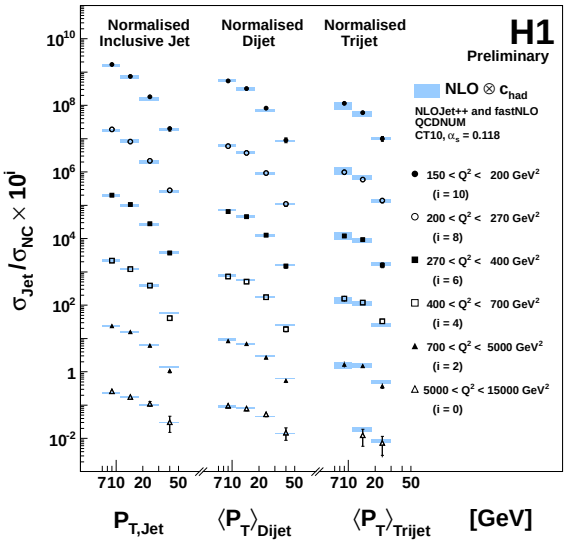

Figure 2: Normalized inclusive jet, dijet and trijet cross sections as functions of virtuality Q^2 and transverse momentum of the leading jet P_T (or average transverse momentum of the leading jets $\langle P_T \rangle$)

$\alpha_S(M_Z)$ is determined to be

$$\alpha_S(M_Z) = 0.1163 \pm 0.0011(exp.) \pm 0.0008(had) \; {}^{+0.0044}_{-0.0035}(th.) \pm 0.0014(PDF)$$

The extracted value is consistent with previous H1 results. The theoretical uncertainties, estimated from scale variations, are significantly larger than the experimental uncertainty.

2.2. Jet production at low Q^2

The data used for the low Q^2 measurement of jet cross sections [3] were recorded with the H1 detector in the years 1999-2000 and the corresponding integrated luminosity is 43.5 pb^{-1}. The kinematic region covered by this analysis is defined by $5 < Q^2 < 100$ GeV^2 and $0.2 < y < 0.7$. The transverse momentum of jets in the Breit frame is required to be above 5 GeV. In addition, the dijet and trijet events are accepted only if the invariant mass M_{12} of the two leading jets exceeds 18 GeV. The measured inclusive, dijet and trijet cross sections as a function of P_T ($\langle P_T \rangle$ for dijet and trijet) and Q^2 are shown in Figure 3. The NLO QCD calculations, corrected for hadronisation effects, provide a good description of the data within the quoted theoretical and experimental uncertainties. The theoretical uncertainties are dominated by the renormalisation scale variation. The higher order calculations, beyond NLO, are needed to improve the theory such that its precision matches the precision of the data. The α_S determination is performed from individual bins of the double differential inclusive jet cross section, $d^2\sigma/dQ^2dP_T$, and the dijet and trijet cross sections, $d^2\sigma/dQ^2d\langle P_T \rangle$. Only those bins are used in which the k-factor is below 2.5. The result from the common fit taking the correlation into account with a fit quality $\chi^2 = 49.8/61$ is:

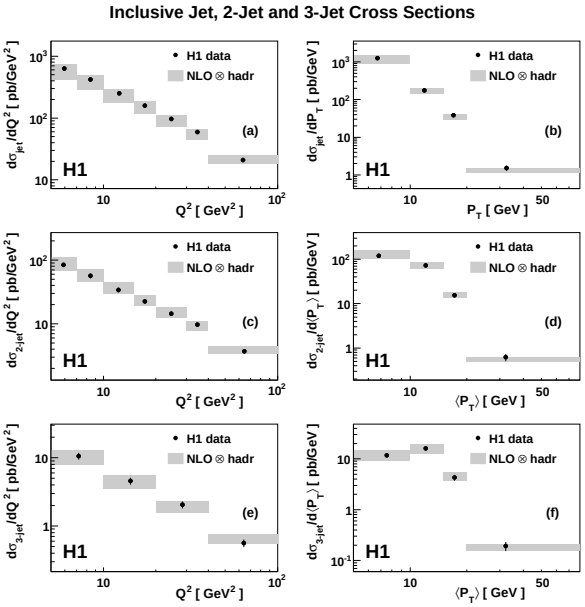

Figure 3: Inclusive jet cross section(a,b), dijet (c,d) and trijet (e,f) cross sections as functions of virtuality Q^2 and transverse momentum of the leading jet P_T (or average transverse momentum of the two leading jets $\langle P_T \rangle$) compared with NLO QCD prediction.

$$\alpha_S(M_Z) = 0.1160 \pm 0.0014(exp.) \; {}^{+0.0093}_{-0.0077}(th.) \pm 0.0016(PDF)$$

The benefit of the simultaneous fit is evident from the Figure 4 where the values of α_S as a function of the renormalisation scale $\mu_r = \sqrt{(Q^2 + P^2_{T,obs})/2}$ are presented for the individual fits to inclusive jet, dijet, trijet cross sections and for the simultaneous fit. The experimental uncertainties are reduced significantly in the case of the combined fit. Also, these results are compared to an earlier H1 jet analysis at the high Q^2 [4]. The low Q^2 measurement together with data from the high Q^2 analysis provides a test of the running of the strong coupling for renormalisation scales μ_r ranging from 6

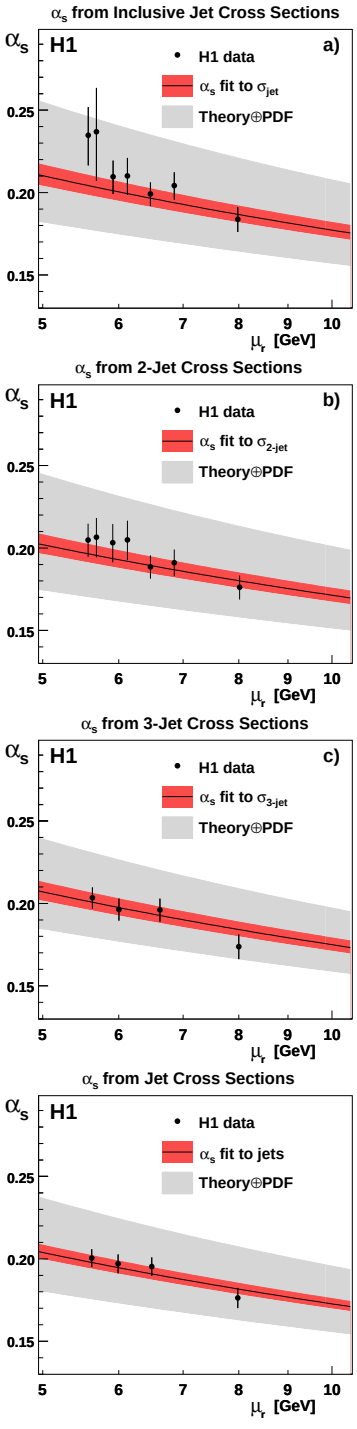

Figure 4: The $\alpha_S(\mu_r = \sqrt{(Q^2 + P^2_{T,obs})}/2)$ values extracted from :(a) inclusive cross section, (b) dijet, (c) trijet and by a simultaneous fit of all jet cross sections (bottom figure) at low Q^2. The solid lines show the two loop solution of the renormalization group equation obtained by evolving the corresponding fitted value of $\alpha_S(M_Z)$.

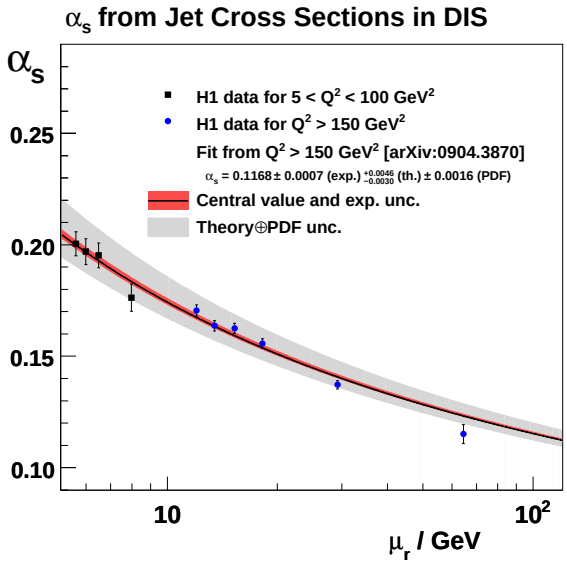

Figure 5: The α_S values as a function of the scale $\mu_r = \sqrt{(Q^2 + P^2_{T,obs})}/2$. The squares show the same low Q^2 results as in Figure 4 (bottom) and the circles present the results of the early H1 jet analysis at high Q^2[4]. The solid line shows the two loop solution of the renormalization group equation obtained by evolving the $\alpha_S(M_Z)$ extracted from the jets at high Q^2 .

to 70 GeV as illustrated in Figure 5. The agreement between the α_S extractions in the different Q^2 regimes is very good.

3. Inclusive jet production in photoproduction

Cross sections for inclusive-jet photoproduction have been measured [5] using data corresponding to an integrated luminosity of 300pb^{-1} collected with the ZEUS detector. The results are given in the kinematic region $Q^2 < 1$ GeV^2 and γp centre-of-mass energies in the region $142 < W_{\gamma p} < 293$ GeV. The jets identified in laboratory frame with the k_T, anti-k_T and SIScone jet algorithms and with jet radius $R = 1$ are required to have the transverse energies $E_T^{jet} > 17$ GeV and the pseudorapidities $-1.0 < \eta^{jet} < 2.5$.

Measurement of the single-differential cross sections based on the k_T jet algorithm as functions of E_T^{jet} and η^{jet} are presented in Figures 6 and 7. The NLO QCD calculation reproduces the dependence on the transverse energy $d\sigma/dE_T^{jet}$ well. The measured pseudorapidity dependence $d\sigma/d\eta_T^{jet}$ is well described for $\eta^{jet} \lesssim 2$, however an excess of data with respect to the theory is observed for large η^{jet} values. The influence of non-perturbative (NP) effects not related to hadronisation

was investigated by using samples of PYTHIA MC program including multiparton interactions with a minimum transverse momentum for the secondary scatter, $p^{sec}_{T,min}$, of 1, 1.5 or 2 GeV. A comparison of these calculations (NLO⊗NP) to the data is shown in Figure 6 and 7. The prediction with $p^{sec}_{T,min} = 1.5$ GeV is closest to the data. These observations indicate the possible presence of effects such as the underlying event in the data, which are not included in the NLO QCD calculation.

Measurements of the inclusive-jet cross sections based on the k_T jet algorithm as functions of E^{jet}_T are presented in Figure 8 for different regions of η^{jet}. The NLO QCD predictions give a good description of the data, except for the region of low E^{jet}_T and high η^{jet}. In particular, for the region $2 < \eta^{jet} < 2.5$, where non-perturbative effects are expected to contribute most, the data are well described only for $E^{jet}_T > 21$ GeV.

Outside the problematic region, the measured cross sections are well reproduced by the NLO calculations using either of th three jet algorithms under investigation: k_T,anti-k_T and SIScone/k_T. In order to compare the jet algorithms in greater details, ratios of the measured cross sections, anti-k_T/k_T, SIScone/k_T and anti-k_T/SIScone were studied. These ratios are shown in Figure 9 and offer the possibility of a stringent test of the description of the differences between jet algorithms due to the partial cancellation of experimental and theoretical uncertainties. The measured ratios are well described by the QCD calculation within the uncertainties, which are dominated by scale uncertainties. The measured single-differential cross sections $d\sigma/dE^{jet}_T$ based on the three jet algorithms were used to determine values of $\alpha_S(M_Z)$. Only the measurements for $E^{jet}_T > 21$ GeV were used in the fit to minimise the influence of possible non-perturbative contributions. In addition,the requirement $E^{jet}_T < 71$ GeV was used because of the relatively large uncertainty originated from the proton PDFs for higher E^{jet}_T values. The values of $\alpha_S(M_Z)$ obtained from the measured $d\sigma/dE^{jet}_T$ are:

$$\begin{aligned}
\alpha_S(M_Z)|_{k_T} &= 0.1206^{+0.0023}_{-0.0022}(exp.)^{+0.0042}_{-0.0035}(th.),\\
\alpha_S(M_Z)|_{anti-k_T} &= 0.1198^{+0.0023}_{-0.0022}(exp.)^{+0.0041}_{-0.0034}(th.),\\
\alpha_S(M_Z)|_{SIS\,cone} &= 0\,.1196^{+0.0022}_{-0.0021}(exp.)^{+0.0046}_{-0.0043}(th.).
\end{aligned}$$

These values are consistent and indicate that the performance of the three jet algorithms is similar. The extracted values of $\alpha_S(M_Z)$ are consistent with other determinations at HERA, as well as with the results obtained in $p\bar{p}$ collisions. The experimental precision is comparable to α_S measurements obtained from e^+e^- experiments. The scale dependence of α_S was studied in Figure 10, where the extracted values α_S are shown as

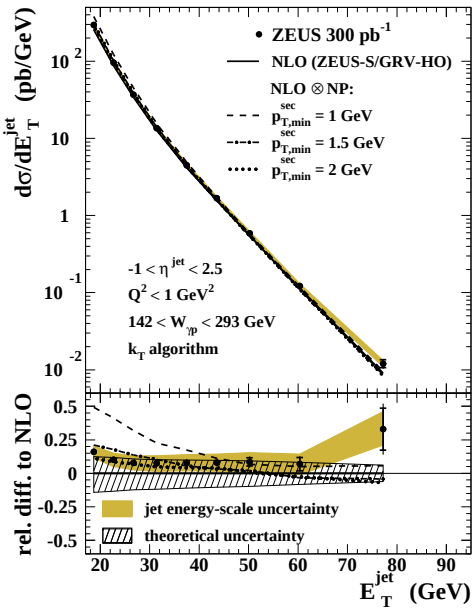

Figure 6: The differential cross section $d\sigma/dE^{jet}_T$ for inclusive jet photoproduction compared to NLO QCD calculations.

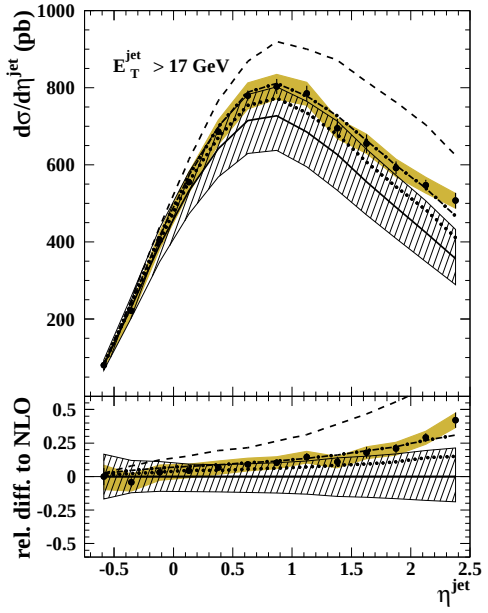

Figure 7: The differential cross section $d\sigma/d\eta^{jet}_T$ for inclusive jet photoproduction compared to NLO QCD calculations.

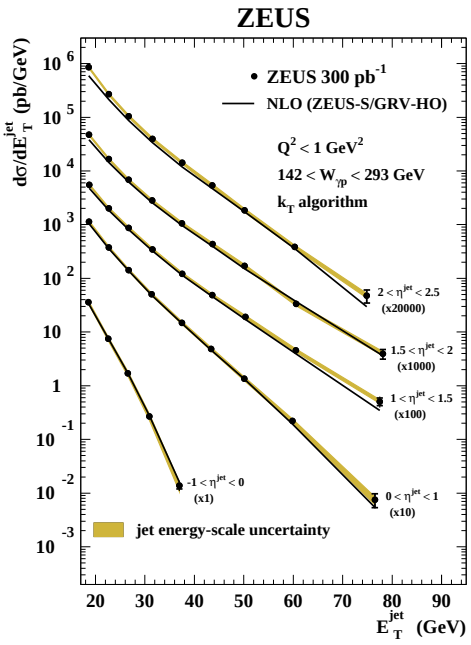

Figure 8: The inclusive jet photoproduction cross section $d\sigma/dE_T^{jet}$ in different regions of η^{jet}. The data are compared to NLO QCD calculations.

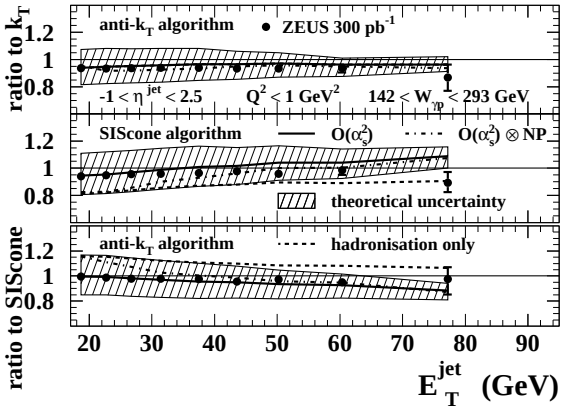

Figure 9: The ratios of the measured cross sections anti-k_T/k_T, SIScone/k_T and anti-k_T/SIScone as a function of E_T^{jet}

a function of E_T^{jet}. The extracted values of α_S as a function of E_T^{jet} are shown in Figure 10. The data demonstrate the running of α_S over a large range in E_T^{jet} in a single experiment. The predicted running of the strong coupling calculated at two loops is in good agreement with data.

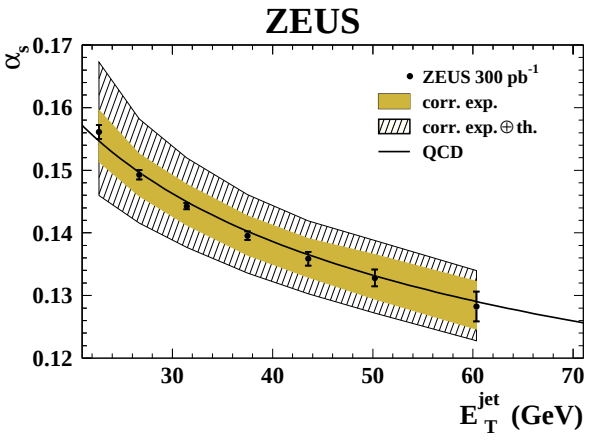

Figure 10: The α_S values determined in each $\langle E_T^{jet} \rangle$ value from the measured $d\sigma/dE_T^{jet}$ cross section using the k_T algorithm. The solid line indicates the QCD prediction at two loops obtained from the corresponding $\alpha_S(M_Z)$ value determined in the presented analysis.

4. Summary of recent $\alpha_S(M_Z)$ determinations

A summary of the $\alpha_S(M_Z)$ determinations given in this document is shown in Figure 11. The obtained values are in good agreement with the word average[6] . The experimental precision is as good as or better than the precision reached in other measurements. however, the measurements of $\alpha_S(M_Z)$ from HERA jet data are dominated by large theoretical uncertainties, which are related to missing higher orders in the calculations.

The inclusion of jet data in a NLO QCD PDF fit analysis with a simultaneous determination of the strong coupling constant $\alpha_S(M_Z)$ significantly reduces the correlation between the gluon parton density function and the strong coupling constant [7]. In addition to the sensitivity to α_S the jet data provide an additional constrain on the gluon density. This is illustrated in Figure 12 and Figure 13 where the results of the fits obtained using $\alpha_S(M_Z)$ as a free parameter are shown for $Q^2 = 10$ GeV^2 [8]. The gluon density has very large uncertainty when inclusive data alone are used. Inclusion of the jet data reduces this uncertainty by about a factor of two and most significantly at low x.

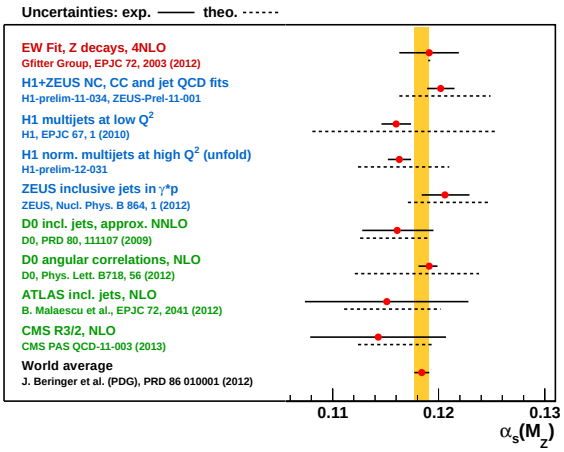

Figure 11: Comparison of the recent values of $\alpha_S(M_Z)$ obtained from the jet production cross sections at HERA, determinations from other experiments and the world average.The shaded band represents the uncertainty of the world average.

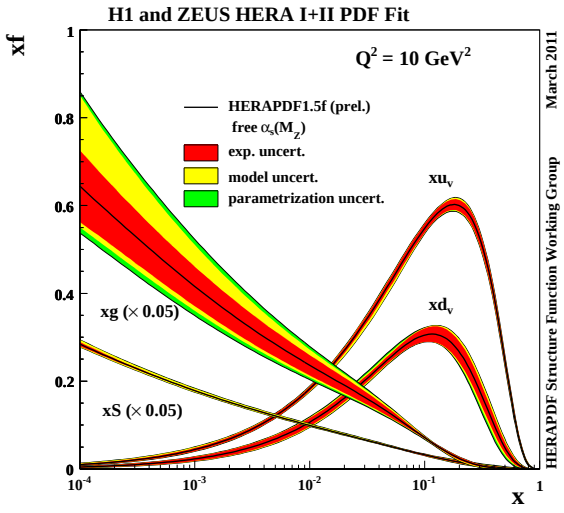

Figure 12: Parton distribution function fit as a function of x for Q^2 = 10 GeV^2 when inclusive data alone are used. The strong coupling $\alpha_S(M_Z)$ is free parameter. The central values of the PDFs (solid line) are shown together with the experimental, model and parametrisation uncertainties by the red, yellow and green shaded bands, respectively.

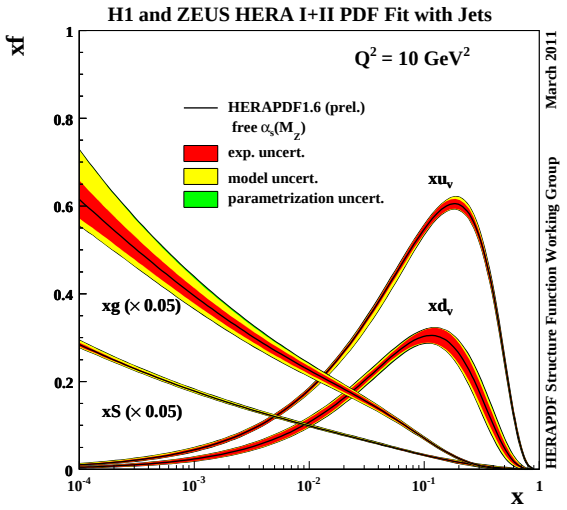

Figure 13: Parton distribution functions for HERAPDF1.6 fit as a function of x for Q^2 = 10 GeV^2 with the addition of jet data. Other details as in the caption to Figure 12.

5. Forward jet azimuthal correlation in DIS

The HERA collider has extended the available kinematic range for DIS to regions of Bjorken x as small as 10^{-5} at Q^2 of a few GeV^2. At the large $\gamma^* p$ centre-of-mass energy available at small x, a transition is expected from parton cascades ordered in transverse momentum, described by DGLAP evolution equations [9], to cascades unordered in transverse momentum, described by the BFKL approach [10]. The CCFM evolution [11] has angular ordering of parton emissions in a scheme which aims to unify the DGLAP and BFKL approaches. Measurements of DIS events with energetic jets of high transverse momentum produced close to the proton direction in the laboratory frame, here referred to as the forward region, are considered to be particularly sensitive to QCD dynamics at low x [12]. The distribution of the azimuthal angle difference, $\Delta\phi$, between the forward jet and the scattered electron is expected to show an increase of the azimuthal angle decorrelation with the electron-jet rapidity distance for evolution schemes without ordering in transverse momentum. The H1 collaboration exploits this idea to test the different QCD evolution mechanisms.

The data used in the analysis were collected with the H1 detector in 2000 and correspond to an integrated luminosity of 38.2 pb^{-1} [13]. The analysis phase space is restricted to: $5 < Q^2 < 85$ GeV^2, $0.0001 < x < 0.004$ and $0.1 < y < 0.7$. Jets are identified using the k_T cluster

algorithm in the Breit frame and then boosted to the laboratory frame. The events analyzed contain at least one forward jet which satisfies the following cuts in the laboratory frame: $P_{T,fwd\,jet} > 6$ GeV and $1.73 < \eta_{fwd\,jet} < 2.79$. In order to enhance the effects of BFKL dynamics and suppress the standard DGLAP evolution additional requirements are applied: $x_{fwd\,jet} = E_{fwd\,jet}/E_p > 0.35$ and $0.5 < P^2_{T,fwd\,jet}/Q^2 < 6$.

The forward jet cross section $d\sigma/d\Delta\phi$ as a function of the azimuthal angle difference $\Delta\phi$ between the most forward jet and the scattered positron is shown in Figure 14 for three intervals of the positron-jet rapidity distance Y, defined as $Y = ln(x_{fwd\,jet}/x)$. The prediction of three QCD-based models with different underlying parton dynamics are compared with data. The cross sections are well described in shape and normalisation by CDM which has a BFKL-like approach. The RAPGAP prediction, which implements DGLAP evolution, falls below the data, particularly at large$Y$. Calculations in the CCFM scheme as implemented in CASCADE using the uPDF set A0 [14] overestimate the measured cross section for large $\Delta\phi$ values in the two lowest Y intervals. However, in the highest Y interval, this model provides a description of the data as good CDM.

At the bottom of Figure14 the ratio plots for normalized cross section $R = (1/\sigma \cdot d\sigma/d\Delta\phi)_{MC}/(1/\sigma \cdot d\sigma/d\Delta\phi)_{data}$ are presented. These ratio plots show that in the analysed phase space region the shape of the $\Delta\phi$ distributions is well described by all MC models, so this observable alone cannot discriminate between different evolution schemes.

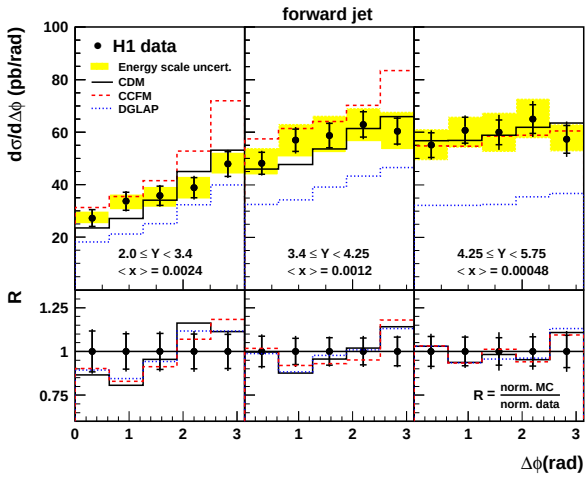

Figure 14: Differential forward jet cross section as a function of the azimuthal angle difference $\Delta\phi$ between the most forward jet and the scattered positron in three intervals of the variable $Y = ln(x_{fwd\,jet}/x)$.

6. Summary

The HERA experiments, H1 and ZEUS, provide high precision measurements of inclusive-jet, dijet and trijet production in DIS and photoproduction. In general, the measurements are described by the perturbative QCD NLO calculations. The strong coupling constant $\alpha_S(M_Z)$ is extracted from jet production data in different kinematic regimes, and is found to be competitive with other experiments in experimental precision. The total precision, however, is limited by theoretical uncertainties. The running of α_S is tested over a wide range of scales. Higher order calculations will be needed to fully exploit the potential of the precision jet data from HERA.

To test parton radiation at low x, cross sections are measured as a function of $\Delta\phi$ and rapidity separation between the forward jet and the scattered positron in DIS. The data are best described by the BFKL-like model CDM, whereas NLO DGLAP predictions using the RAPGAP generator are below the data in normalisation. Somewhat surprising, the shape as a function of $\Delta\phi$ is found to have little discriminating power.

References

[1] H1 Collaboration, preliminary result: H1prelim-11-032, 2011, H1 Collaboration, preliminary result: H1prelim-12-031, 2012.

[2] M. Cacciari and G. P. Salam, Phys. Lett. B **641** (2006) 57 [hep-ph/0512210].

[3] F. D. Aaron *et al.* [H1 Collaboration], Eur. Phys. J. C **67** (2010) 1 [arXiv:0911.5678 [hep-ex]].

[4] F. D. Aaron *et al.* [H1 Collaboration], Eur. Phys. J. C **65** (2010) 363 [arXiv:0904.3870 [hep-ex]].

[5] H. Abramowicz *et al.* [ZEUS Collaboration], Nucl. Phys. B **864** (2012) 1 [arXiv:1205.6153 [hep-ex]].

[6] J. Beringer *et al.* [Particle Data Group Collaboration], Phys. Rev. D **86** (2012) 010001.

[7] Talk by A. Geiser for the H1 and ZEUS Collaboration, these Proceedings.

[8] H1 Collaboration, preliminary result: H1prelim-11-034, 2011, ZEUS Collaboration, preliminary result: ZEUS-prel-11-001, 2011.

[9] V. Gribov and L. Lipatov, Sov. J. Nucl. Phys. **15** (1972) 438 and 675; L. Lipatov, Sov. J. Nucl. Phys. **20** (1975) 94; Nucl. Phys. **B 126** (1977) 298; Y. Dokshitzer, Sov. Phys. JETP **46** (1977) 641.

[10] E. Kuraev, L. Lipatov and V. Fadin, Sov. Phys. JETP **44** (1976) 443; E. Kuraev, L. Lipatov and V. Fadin, Sov. Phys. JETP **45** (1977) 199; Y. Balitsky and L. Lipatov, Sov. J. Nucl. Phys. **28** (1978) 822.

[11] M. Ciafaloni, Nucl. Phys. **B 296**, (1988) 49; S. Catani, F. Fiorani and G. Marchesini, Phys. Lett. **B 234** (1990) 339; S. Catani, F. Fiorani and G. Marchesini, Nucl. Phys. **B 336** (1990) 18.

[12] A. H. Mueller, Nucl. Phys. B (Proc. Suppl.) **18 C** (1990) 125.

[13] F. D. Aaron *et al.* [H1 Collaboration], Eur. Phys. J. C **72** (2012) 1910 [arXiv:1111.4227 [hep-ex]].

[14] H. Jung, in "Proceedings of the XII International Workshop on Deep Inelastic Scattering (DIS2004)", eds. D. Bruncko, J. Ferencei, P. Strížencec, (2004), p.299 [hep-ph/0411287].